

Supplementary Material

Fabrication of a heterovalent dual-cation pre-embedded hydrated vanadium oxide cathode for high-performance zinc ion storage

Wei Liu^a, Xiaoyu Liu^{a,}, Fanghua Ning^a, Sidra Subhan^b, Yuyu Liu^a, Qian Li^c, Jiujun Zhang^a, Shigang Lu^a, Jin Yi^{a,*}*

^a Department of Chemistry & Institute for Sustainable Energy, Shanghai University, Shanghai 20044, China.

^b Department of Chemistry, Bacha Khan University Charsadda, 24420, KPK, Pakistan.

^c College of Materials Science and Engineering, National Engineering Research Center for Magnesium Alloys, Chongqing University, Chongqing 400044, China.

* Corresponding authors

E-mail address: xiaoyuli@shu.edu.cn (X. Liu), jin.yi@shu.edu.cn (J. Yi).

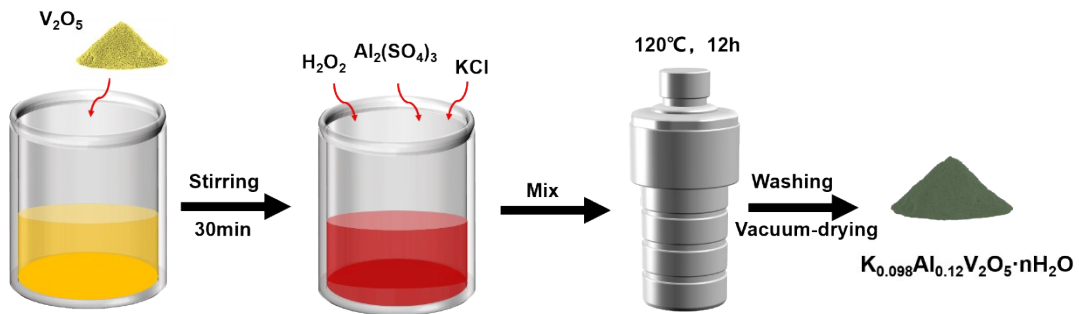


Fig. S1. Schematic illustration of preparation process of KAlVOH cathode material.

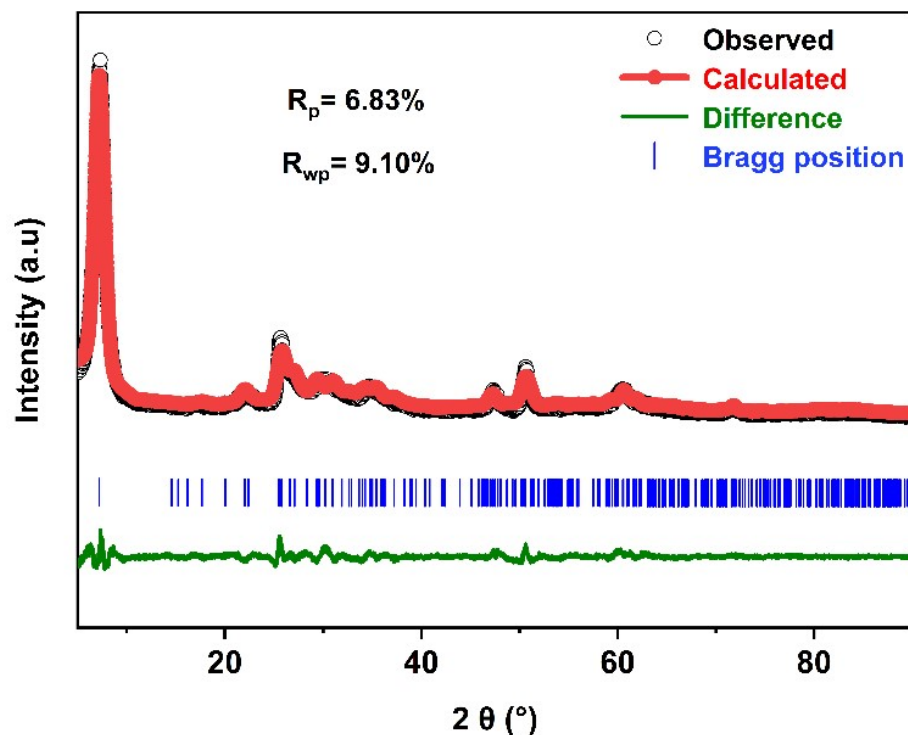


Fig. S2. The XRD Rietveld refinement patterns of KAlVOH.

Table S1 The lattice parameters of KAIVOH.

	<i>a</i> (Å)	<i>b</i> (Å)	<i>c</i> (Å)	α (°)	β (°)	γ (°)	<i>V</i> (Å ³)
KAIVOH	11.57	3.60	12.09	90	96.25	90	500.67
Atom	Position	Occupancy	x	y	z		
O1	4i	0.907249	0.067908	0.000000	0.056304		
V1	4i	0.952933	0.573328	0.000000	0.149726		
O5	4i	1.000000	0.329173	0.000000	0.243342		
O6	4i	0.782890	0.105561	0.000000	0.473414		
V2	4i	0.820367	0.271684	0.000000	0.114128		
O4	4i	1.000000	0.571255	0.000000	0.298481		
O2	4i	0.960103	0.442318	0.000000	0.123395		
O3	4i	1.000000	0.744282	0.000000	0.001505		
K	2c	0.098000	0.000000	0.000000	0.500000		
Al	2c	0.120000	0.000000	0.000000	0.500000		

Table S2 Correlation between properties of the preintercalated M cations (size and electronegativity) and the interplanar spacing of $M_xV_2O_5 \cdot nH_2O$ materials in this work¹⁻⁶.

Preintercalated M cation	K/Al	Li	Na	K	Al
Ionic radius Å	-	0.76	0.95	1.33	0.53
Hydrated ion Radis Å	-	3.82	3.58	3.31	4.8
Interplanar spacing Å	13.2	12.0	11.0	9.9	13.36
reported in this paper					
Electronegativity of element (Pauling scale)	-	1.0	0.93	0.82	1.61
Electronegativity difference with O (3.44)	-	2.44	2.51	2.62	1.83

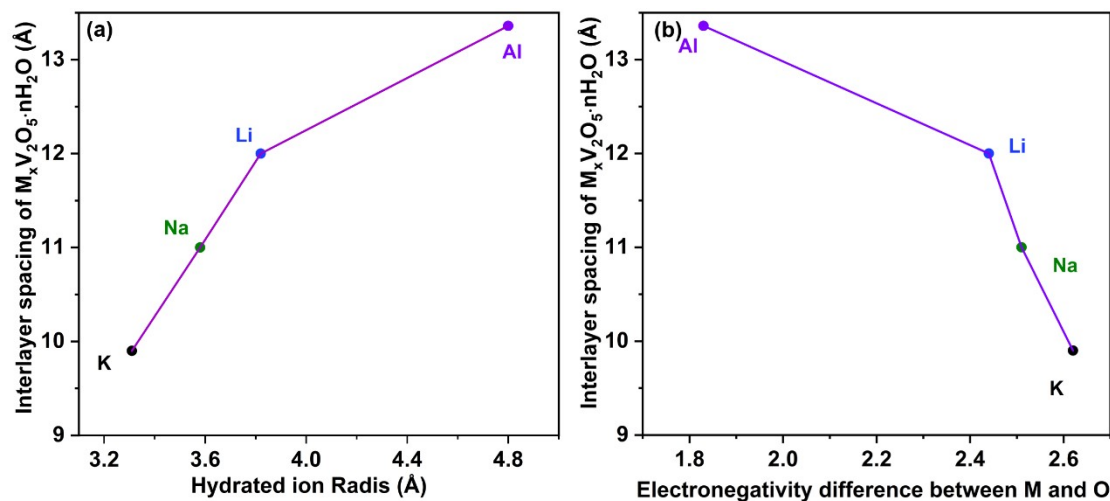


Fig. S3. The relationship between interlayer spacing of $M_xV_2O_5 \cdot nH_2O$ (reported in this paper) with respect to the (a) radius of the hydrated M cation and (b) electronegativity difference between M and oxygen.

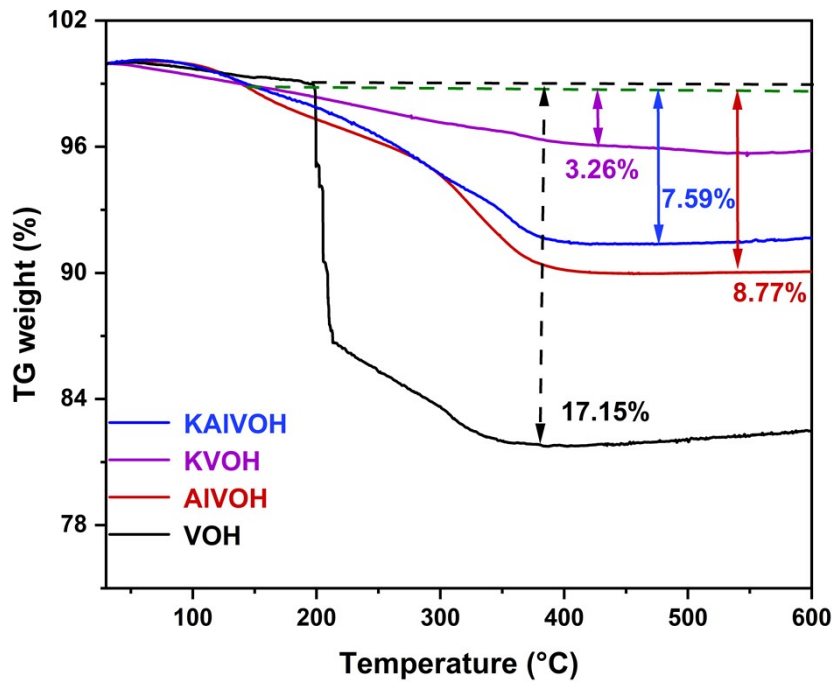


Fig. S4. TG curves of KAlVOH, KVOH, AlVOH and VOH materials.

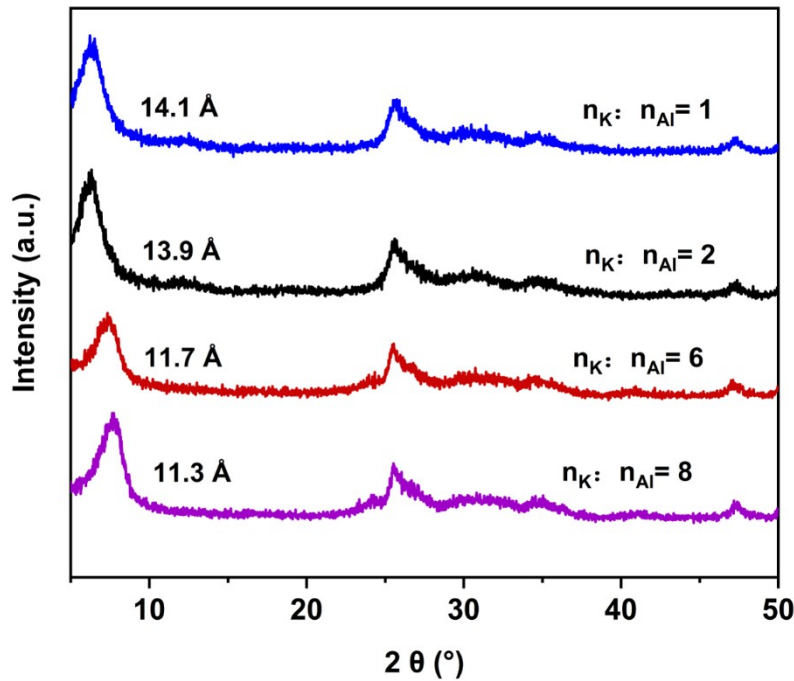


Fig. S5. XRD patterns of KAlVOH with various K^+/Al^{3+} molar ratios of 1, 2, 6 and 8.

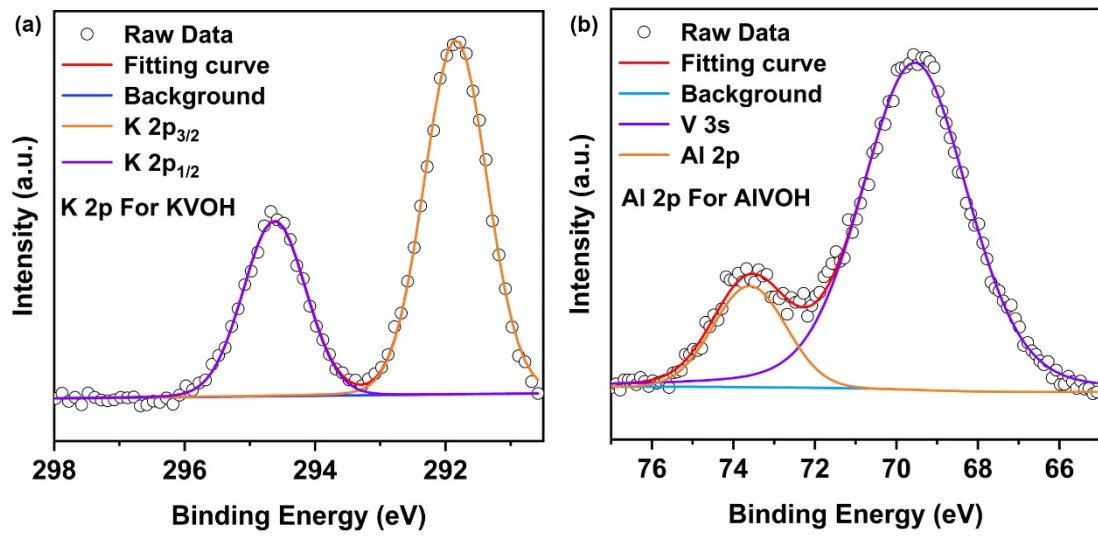


Fig. S6. High-resolution XPS spectra of (a) K 2p for KVOH material and (b) Al 2p for AlVOH material.

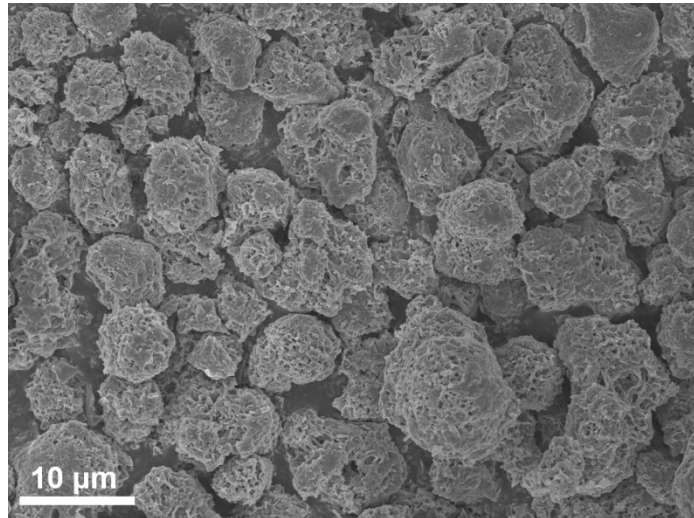


Fig. S7. Low-magnification SEM image of KAIVOH material.

Table S3 Atomic ratio of K, Al and V in KAIVOH by ICP analysis.

Element	ratio
K : Al : V	0.098 : 0.12 : 2

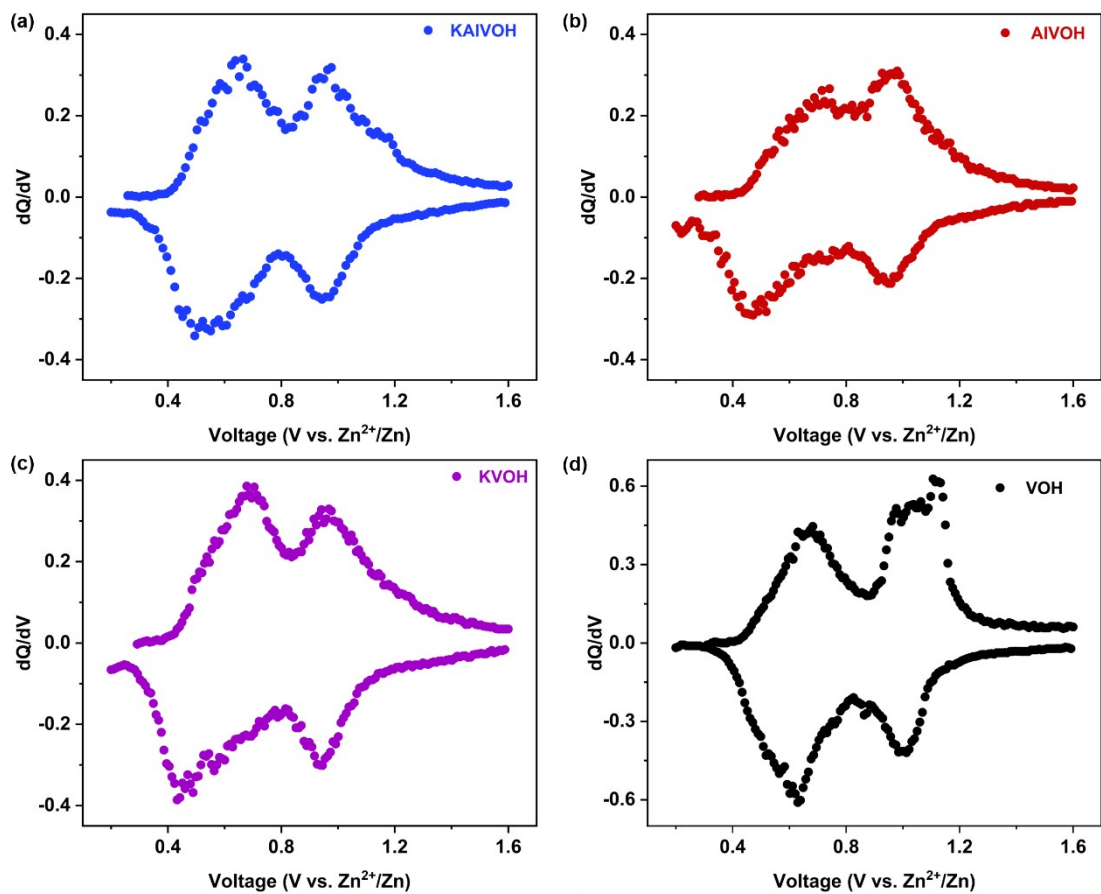


Fig. S8. The differential capacity curves of (a) KAlVOH, (b) AlVOH, (c) KVOH, (d) VOH cathode materials at 0.05 A g^{-1} .

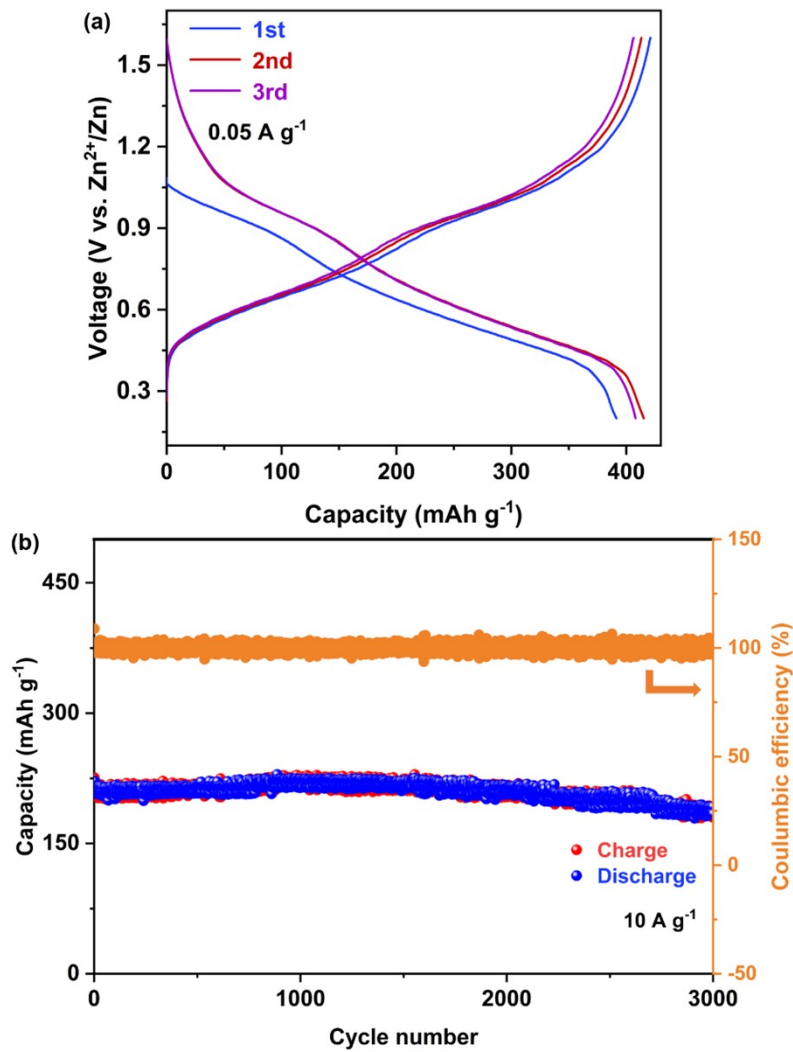


Fig. S9. Electrochemical properties of KAlVOH cathode material: (a) voltage profiles at 0.05 A g^{-1} in the initial three cycles; (b) Cycling performance at 10 A g^{-1} .

Table S4 Performance comparison of selected V-based cathode materials of ZIBs.

Materials	Specific capacity / mAh g ⁻¹ (Current density: A g ⁻¹)	Cycle numbers (Current density: A g ⁻¹)	Capacity retention	Ref.
CaVOH/rGO	409 (0.05)	2000 (4)	90%	4
H ₁₁ Al ₂ V ₆ O _{23.2} @graphene	305.4 (1)	900 (5)	94%	5
Na _{0.33} V ₂ O ₅	367.1 (0.1)	1000 (5)	93%	7
KVO NBs	361 (0.2)	2000 (5)	90.3%	8
NaCa _{0.6} V ₆ O ₁₆ ·3H ₂ O	347 (0.1)	2000 (2)	94%	9
LPVO	377 (0.1)	800 (5)	94%	10
KMgVOH	423 (0.1)	2000 (4)	72%	11
Na-V ₂ O ₅	306 (0.1)	1000 (2)	83.4%	12
KAlVOH	424 (0.05)	3000 (5)	96%	This work

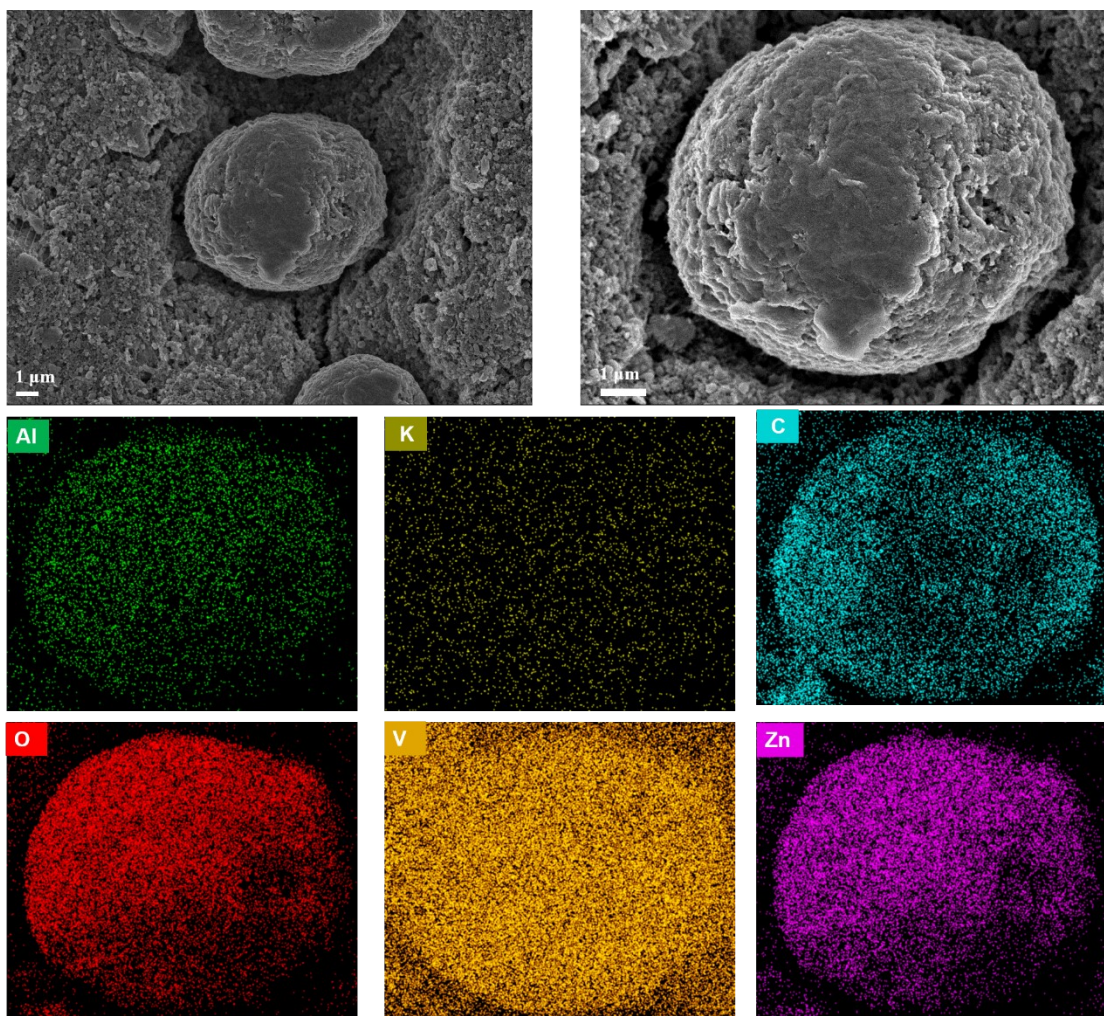


Fig. S10. SEM and EDS element mapping images of KAlVOH cathode material after 3000 cycles.

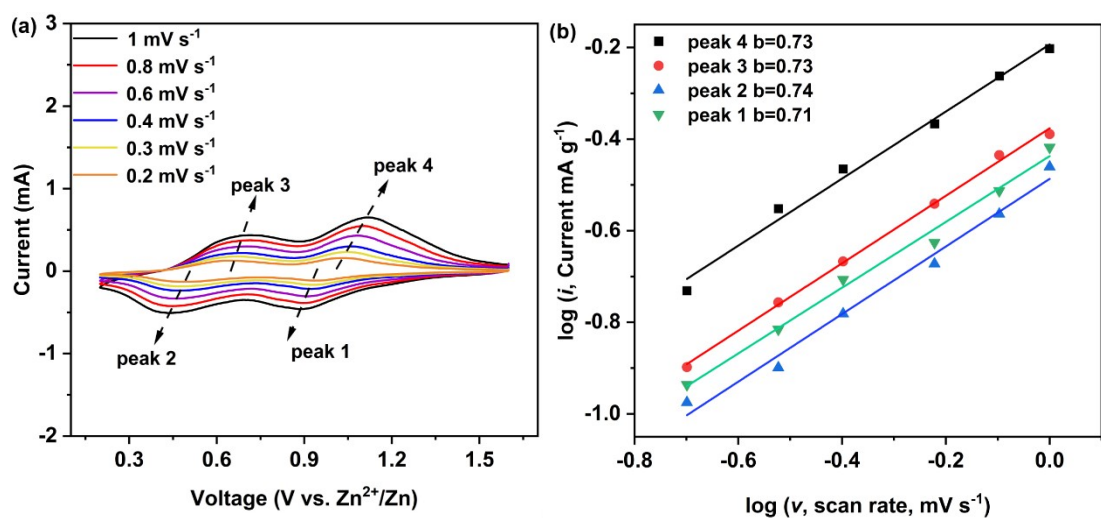


Fig. S11. (a) CV curves at various sweep rates and (b) the relationship between peak currents and sweep rates of the VOH cathode.

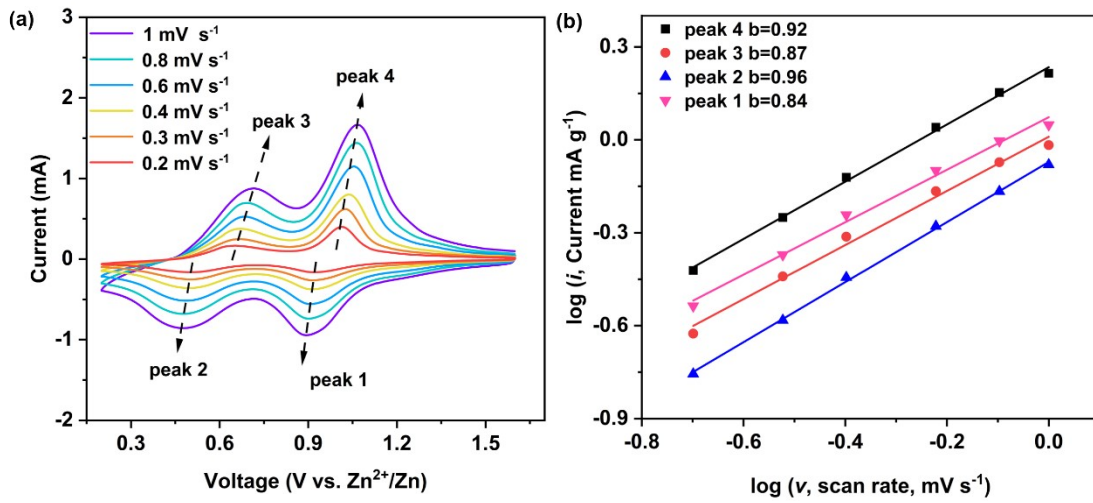


Fig. S12. (a) CV curves at various sweep rates and (b) the relationship between peak currents and sweep rates of the AlVOH cathode.

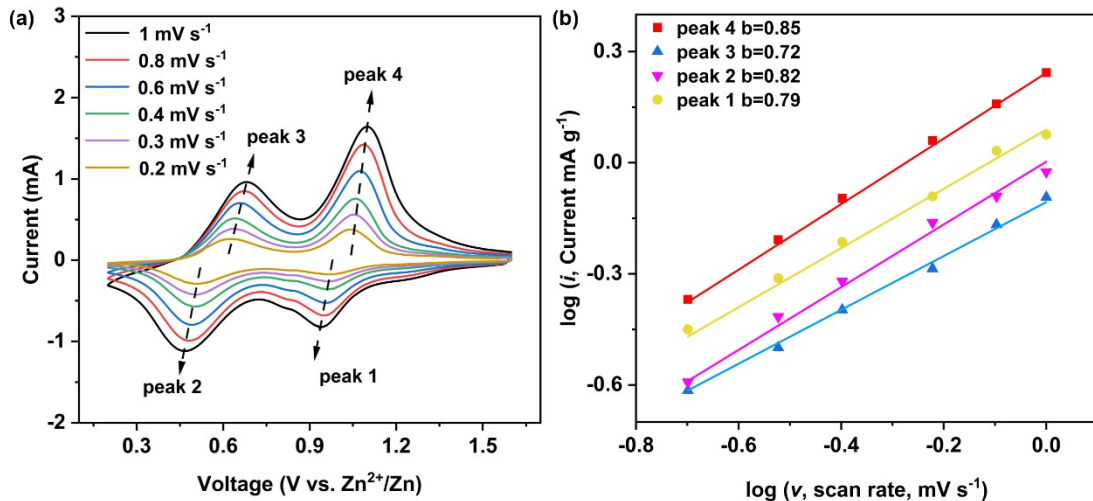


Fig. S13. (a) CV curves at various sweep rates and (b) the relationship between peak currents and sweep rates of the KVOH cathode.

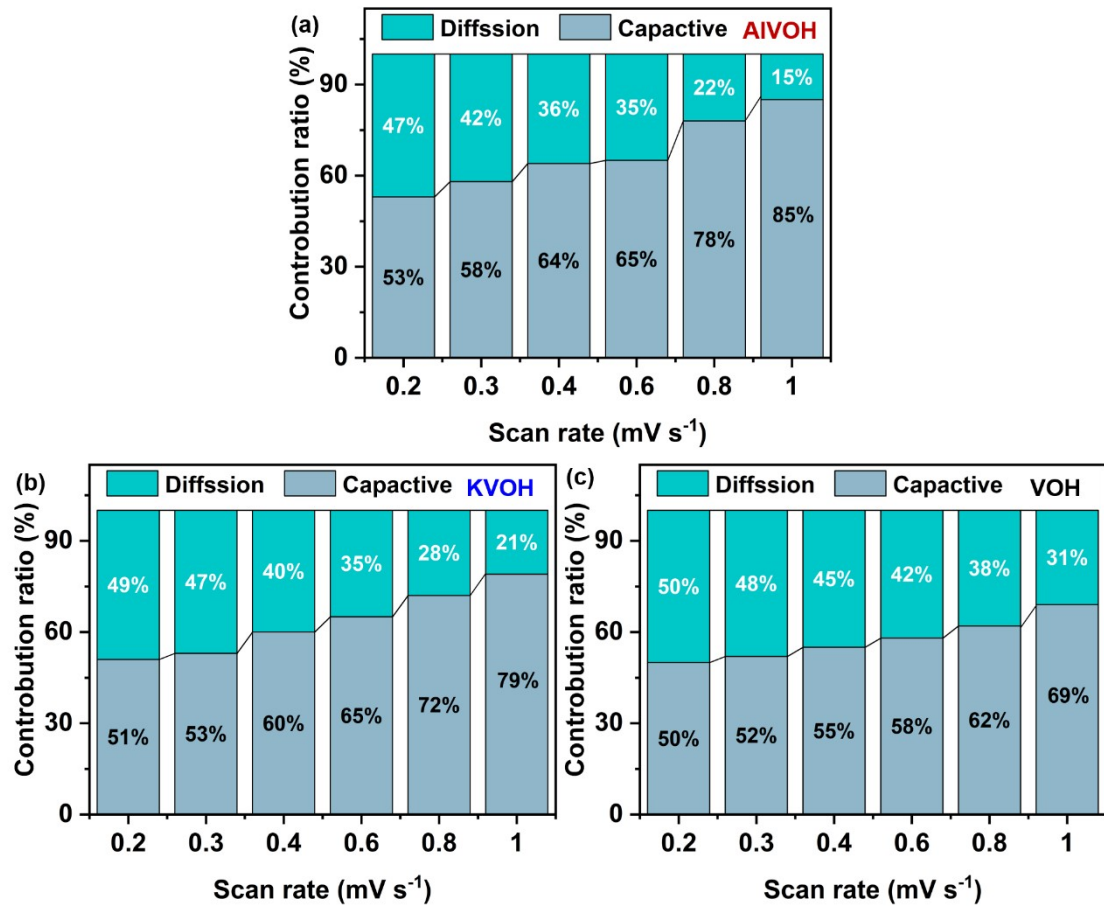


Fig. S14. Contribution ratios of capacity on capacitive contribution and diffusive contribution of the (a) AlVOH, (b) KVOH and (c) VOH cathode materials.

Table S5 The fitting results of distinct resistance elements for VOH, KVOH, AlVOH and KAIVOH cathode materials.

Material	R_s (Ω)	R_{ct} (Ω)
VOH	2.814	760.9
KVOH	1.136	225.7
AlVOH	1.361	134.4
KAIVOH	0.77243	77.03

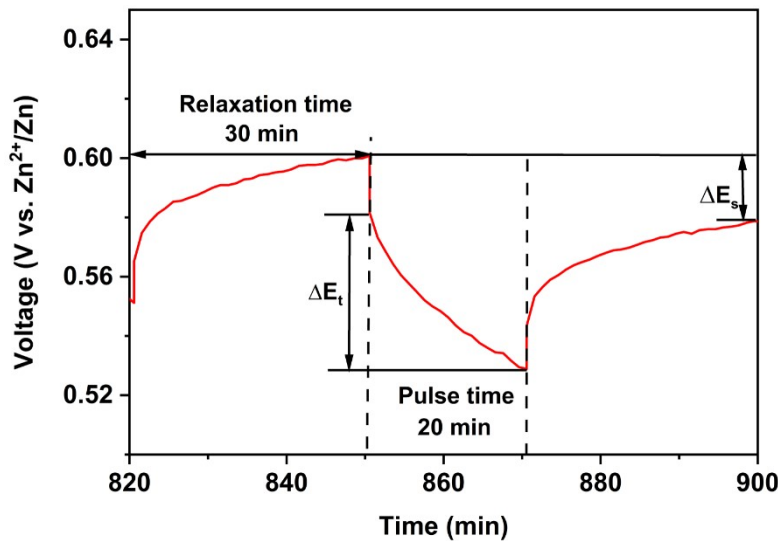


Fig. S15. Schematic illustration of a single step of the GITT during discharge process.

The GITT (Galvanostatic Intermittent Titration Technique) was used to thoroughly investigate the kinetics of solid-state diffusion in the electrode. The solid-state diffusion coefficient of zinc-ion was calculated using the following equation.

$$D_{\text{zn}^{2+}} = \frac{4}{\pi \tau} \left(\frac{n_M V_M}{S} \right)^2 \left(\frac{\Delta E_s}{\Delta E_t} \right)^2$$

In this formula, V_M ($\text{cm}^3 \text{ mol}^{-1}$), n_M (g mol^{-1}) are the molar volume and the molar mass of the VOH, KVOH, AlVOH, KAIVOH cathodes, respectively. And τ (s) is constant current pulse duration and S (cm^{-2}) is the contact area between electrolytes. In addition, E_s is the steady-state voltage change measured by a single-step GITT, and E_t is the voltage change over the duration of

one discharge/charge pulse, independent of the IR drop. As shown in Fig. S11, during the GITT test, discharge or charge the battery at a current rate of 50 mA g^{-1} for 20 minutes, then leave the circuit open for 30 minutes to allow the battery to relax to equilibrium.

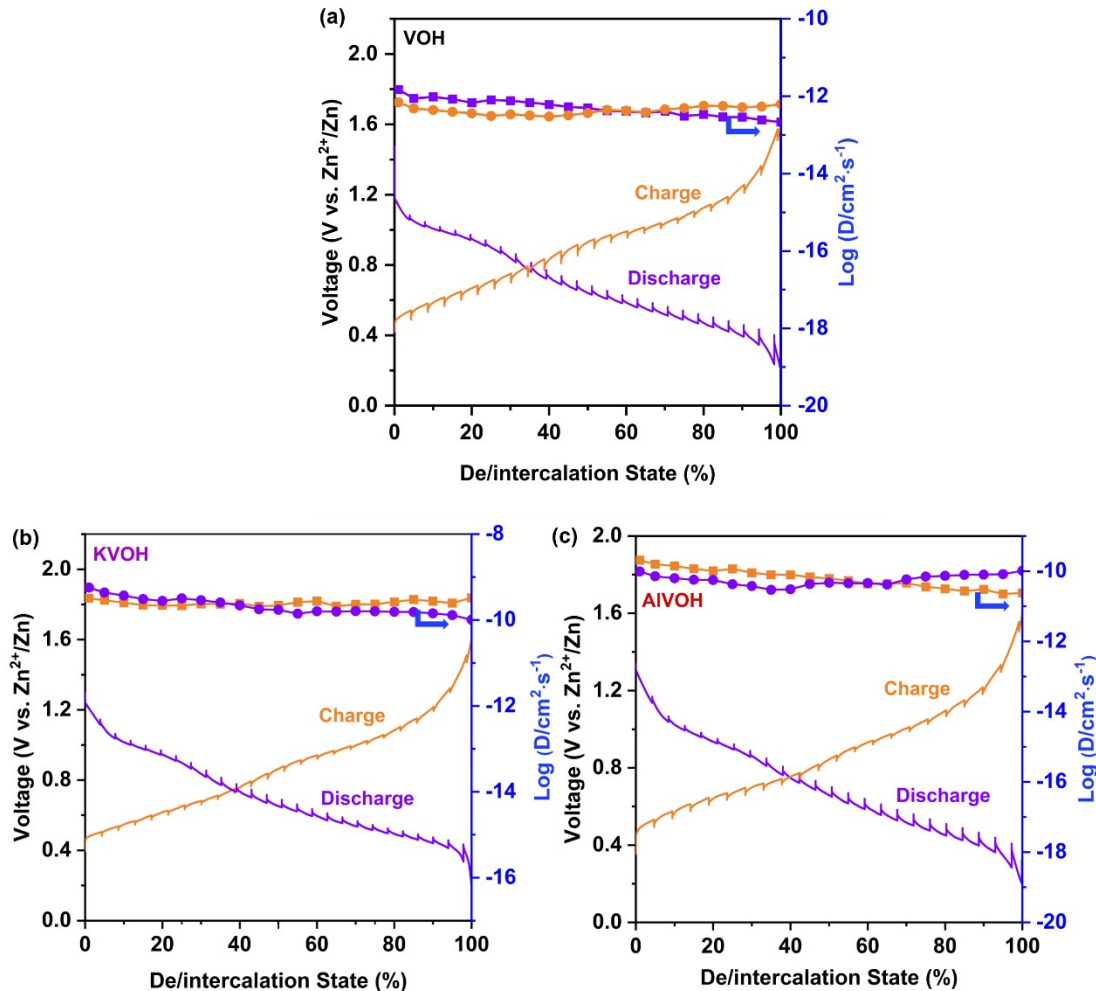


Fig. S16. Galvanostatic intermittent titration technique (GITT) curves at the current density of 0.05 A g^{-1} and the corresponding Zn^{2+} diffusion coefficients of the (a) VOH, (b) KVOH and (c) AlVOH cathode materials.

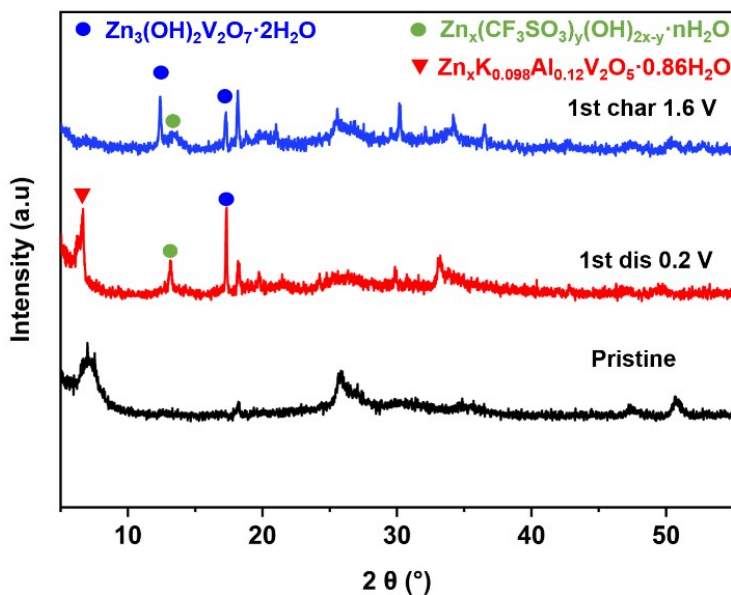


Fig. S17. The *ex situ* XRD patterns of KAlVOH cathode material at various states at $0.1 \text{ A}\cdot\text{g}^{-1}$.

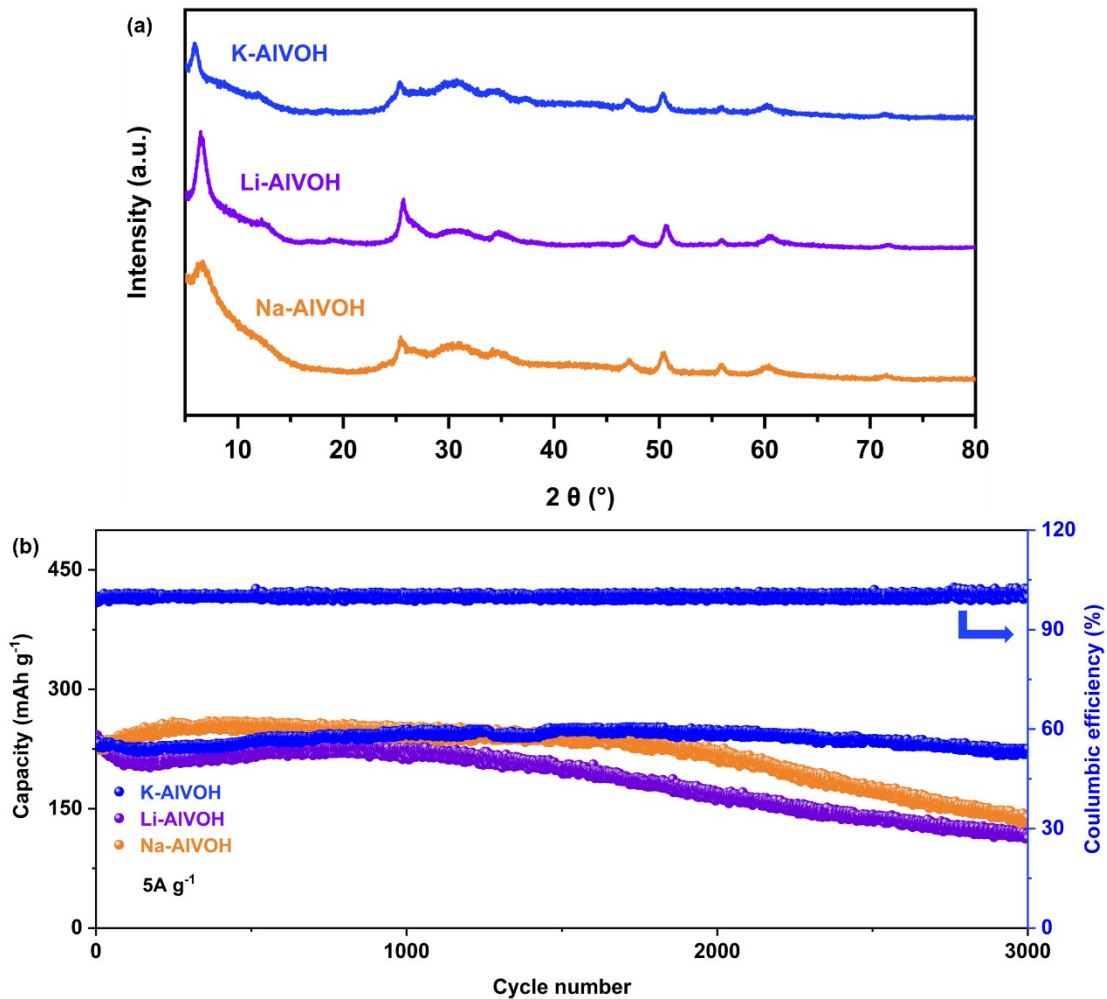


Fig. S18. (a) XRD patterns of KAlVOH, NaAlVOH, and LiAlVOH cathode materials and (b)

cycling performance of three cathode materials at 5 A g⁻¹.

References

1. M. Tian, C. Liu, J. Zheng, X. Jia, E. P. Jahrman, G. T. Seidler, D. Long, M. Atif, M. Alsalhi and G. Cao, *Energy Storage Materials*, 2020, **29**, 9-16.
2. A. G. Volkov, S. Paula and D. W. Deamer, *Bioelectrochemistry and Bioenergetics*, 1997, **42**, 153-160.
3. H. Ma, H. Chen, Y. Hu, B. Yang, J. Feng, Y. Xu, Y. Sun, H. Cheng, C. Li, X. Yan and L. Qu, *Energy & Environmental Science*, 2022, **15**, 1131-1143.
4. W. He, C. Meng, Z. Ai, D. Xu, S. Liu, Y. Shao, Y. Wu and X. Hao, *Chemical Engineering Journal*, 2023, **454**, 140260.
5. W. Zhang, S. Liang, G. Fang, Y. Yang and J. Zhou, *Nano-Micro Letters*, 2019, **11**, 69.
6. X. Jia, R. Tian, C. Liu, J. Zheng, M. Tian and G. Cao, *Materials Today Energy*, 2022, **28**, 101063.
7. T. Hu, Z. Feng, Y. Zhang, Y. Liu, J. Sun, J. Zheng, H. Jiang, P. Wang, X. Dong and C. Meng, *Inorganic Chemistry Frontiers*, 2021, **8**, 79-89.
8. P. He, G. Zhang, X. Liao, M. Yan, X. Xu, Q. An, J. Liu and L. Mai, *Advanced Energy Materials*, 2018, **8**, 1702463.
9. K. Zhu, T. Wu and K. Huang, *Advanced Energy Materials*, 2019, **9**, 1901968.
10. W. He, Z. Fan, Z. Huang, X. Liu, J. Qian, M. Ni, P. Zhang, L. Hu and Z. Sun, *Journal of Materials Chemistry A*, 2022, **545**, 231920.
11. Z. Feng, Y. Zhang, J. Sun, Y. Liu, H. Jiang, M. Cui, T. Hu and C. Meng, *Chemical Engineering Journal*, 2022, **433**, 133795.
12. M. Liu, Z. Li and Y. Zhang, *Journal of The Electrochemical Society*, 2023, **170**, 110524.